

Effect of global momentum conservation on longitudinal flow decorrelation

Pingal Dasgupta,^{1,2} Han-Sheng Wang,^{1,2} and Guo-Liang Ma^{1,2,*}

¹*Key Laboratory of Nuclear Physics and Ion-beam Application (MOE),
Institute of Modern Physics, Fudan University, Shanghai 200433, China*

²*Shanghai Research Center for Theoretical Nuclear Physics,
NSFC and Fudan University, Shanghai 200438, China*

We calculate the longitudinal flow decorrelation coefficients, i.e., $r_n(\eta, \eta_r)$ for $n = 2, 3$, in presence of hydro-like flow and the global momentum conservation (GMC) constraint. We find that the longitudinal flow decorrelation is weakened due to the GMC constraint. The GMC effect is sensitive to the total number of particles involved in the GMC, the average longitudinal momentum and the reference pseudorapidity. Our results of $r_2(\eta, \eta_{rA})/r_2(\eta, \eta_{rB})$ ratio between two reference pseudorapidity bins are consistent with the experimental measurements. We predict that the modification effect of GMC on longitudinal flow decorrelation is stronger at RHIC energies than at LHC energies. Our finding provides a new perspective for understanding the longitudinal flow decorrelation in relativistic heavy-ion collisions.

I. INTRODUCTION

Experiments at the relativistic heavy-ion colliders create excellent opportunities to study the hot and dense deconfined phase of quarks and gluons, commonly known as the QGP (Quark-Gluon Plasma) [1–4]. The azimuthal anisotropic flow of hadrons in heavy ion collisions serves as a key evidence for collective expansion. The relativistic viscous hydrodynamical framework thus has been emerged as the most successful description of the fireball evolution [5–17]. For the past two decades, the flow behaviour has been studied extensively to understand the initial states of the collisions and the transport properties of the strongly interacting medium [18–28].

The anisotropic flow parameters depict the harmonic modulation of the particle density distribution along the azimuthal direction, i.e., $dN/d\phi \propto 1 + 2 \sum_{n=1}^{\infty} v_n \cos[n(\phi - \psi_n)]$, where v_n characterizes the strength of the n th order of anisotropic flow and ψ_n is the corresponding event plane angle. The boost invariant hydrodynamical framework particularly has been very successful in predicting the behaviour of flow observable (i.e., v_n) of different hadrons and their relative fluctuations at mid-rapidity for various symmetric collision systems (A+A) at the Relativistic Heavy Ion Collider (RHIC) and the Large Hadron Collider (LHC)[29]. However, recent developments in the theory and experiments have shown that we require a more realistic 3+1 hydrodynamic framework with fluctuating 3D initial conditions to describe the copious production of particles and their flow observables along the rapidity direction [30–33]. The experiments incorporating various asymmetric and small collisions at both RHIC and the LHC have witnessed the breaking of flow factorisation in both transverse momentum and rapidity directions [34]. The measured observable related to the breaking of flow factorisation in the rapidity direction is called the longitudinal flow decorrelation coefficient (i.e., $r_n(\eta, \eta_r)$), which provides the important insights regarding the longitudinal structure of the fireball produced in heavy-ion collision ($v_n(\eta_1) \neq v_n(\eta_2)$ and $\psi_n(\eta_1) \neq \psi_n(\eta_2)$ for $\eta_1 \neq \eta_2$) [35–37]. For example, both the CMS collaboration and the ATLAS collaboration have measured the longitudinal flow decorrelation coefficients for Pb+Pb and p+Pb collisions for different centrality bins at 2.76A TeV and 5.02A TeV [38, 39]. The ATLAS collaboration has also studied the system size dependence of the longitudinal flow decorrelation coefficients with Xe+Xe collisions at 5.44A TeV [40]. The STAR collaboration has taken a similar initiative to study the coefficients for Au+Au at different beam energies [41], for Ru+Ru and Zr+Zr collisions at 0.2 A TeV [42]. The physical reason of such longitudinal flow decorrelation is thought to be due to the twist of event plane angles of initial torqued fireball [43, 44] or initial-state longitudinal fluctuations [45–47]. The initial spatial decorrelation in the longitudinal direction is finally transferred into the measured longitudinal flow decorrelation through final state evolution [48–52].

The longitudinal flow decorrelation coefficient measures the correlation between two flow vectors at two symmetric rapidity bins. The absence of collectivity in an expanding system produces maximum decorrelation ($r_n(\eta, \eta_r) \approx 0$), whereas, the boost invariant type of longitudinal flow invokes maximum correlation (or minimum decorrelation). There exists an additional source of correlation, called as the “non flow” contribution. The momentum conservation is one of the sources of “non-flow” [53–55], which must be satisfied by final state interactions. Considering the transverse momentum conservation (TMC) and hydro-like flow, the multi-particle cumulants at mid-rapidity have been studied

*glma@fudan.edu.cn

elaborately in the Refs. [56–58]. It has been found that for small collision systems, the non-flow contribution from the TMC cannot be omitted in order to extract the true flow contribution since it is very significant. The boost invariance is not a realistic way to deal 3D expansion, since the initial state fluctuations along the rapidity play an important role in the outcome of the flow coefficients. In this paper, we aim to explore the contribution of global momentum conservation (GMC) on the longitudinal flow decorrelation.

Our paper is organized as follows. In Section II, we derive the two-particle azimuthal correlation under the influence of the GMC. The Section III is dedicated to find out the longitudinal flow decorrelation parameter $r_n(\eta, \eta_r)$ in presence of hydro-like flow and GMC. The Section IV discusses a parametric form of particle production from 3D ideal hydrodynamic evolution. We present our main results about the effects of global momentum conservation on longitudinal flow decorrelation in the Section V. Finally we summarize in Section VI.

II. TWO-PARTICLE AZIMUTHAL CUMULANT FROM GMC

For a system consisting N number of particles, the N -particle joint probability distribution function upon full phase-space integration normalizes to unity. Any M -particle observable ($M < N$) is calculated using M -particle joint probability distribution function in momentum space, which is expressed as $f(\mathbf{p}_1, \mathbf{p}_2, \mathbf{p}_3, \dots, \mathbf{p}_M)$ [53–55]. The M -particle joint probability distribution can simply be expressed as the product of M -single particle distributions, if the M -momenta are independent of each other. However, in reality, the momenta are not independent of each other, consequently, the joint probability distribution function includes extra terms. For 2 and 3-particle cases, the joint probability distributions look as follows :

$$\begin{aligned} f(\mathbf{p}_1, \mathbf{p}_2) &= f_c(\mathbf{p}_1)f_c(\mathbf{p}_2) + f_c(\mathbf{p}_1, \mathbf{p}_2) \\ f(\mathbf{p}_1, \mathbf{p}_2, \mathbf{p}_3) &= f_c(\mathbf{p}_1)f_c(\mathbf{p}_2)f_c(\mathbf{p}_3) + f_c(\mathbf{p}_3)f_c(\mathbf{p}_1, \mathbf{p}_2) + f_c(\mathbf{p}_2)f_c(\mathbf{p}_1, \mathbf{p}_3) + \\ & f_c(\mathbf{p}_1)f_c(\mathbf{p}_2, \mathbf{p}_3) + f_c(\mathbf{p}_1, \mathbf{p}_2, \mathbf{p}_3) \quad , \end{aligned} \quad (1)$$

where, each term is a cumulant corresponding to distinct partition of M -particles. Here, the single particle cumulant corresponds to the single particle probability distribution function, i.e., $f_c(\mathbf{p}) = f(\mathbf{p})$ and the product of single particle cumulant is known as the “indirect” correlation term whereas the M -particle cumulant (i.e., $f_c(p_1, p_2, \dots, p_M)$) represents the “direct” correlation term of M -particles.

In Ref [54, 55], a systematic way of obtaining the cumulants using generating function has been presented. First, we define the generating function of joint probability distribution as follows:

$$G(x_1, x_2, \dots, x_N) = 1 + x_1 f(\mathbf{p}_1) + x_2 f(\mathbf{p}_2) + \dots + x_1 x_2 f(\mathbf{p}_1, \mathbf{p}_2) + \dots \quad (2)$$

where, x_1, x_2, \dots, x_N are auxiliary variables. To obtain the “direct” cumulant terms, we take the logarithm of Eq. (2):

$$\ln G(x_1, x_2, \dots, x_N) = 1 + x_1 f_c(\mathbf{p}_1) + x_2 f_c(\mathbf{p}_2) + \dots + x_1 x_2 f_c(\mathbf{p}_1, \mathbf{p}_2) + \dots, \quad (3)$$

where the coefficient of x_1, x_2, \dots, x_j represents the corresponding cumulant term $f_c(\mathbf{p}_1, \mathbf{p}_2, \mathbf{p}_3, \dots, \mathbf{p}_j)$.

A. Two-particle cumulant from GMC

The momentum conservation is one such constraint that restricts the momentum of particles to be not independent of each other. Next, we discuss how momentum conservation changes the joint probability distribution function. In the centre of mass frame for a N particle system, the sum of N -momenta is always zero, i.e., $\mathbf{p}_1 + \mathbf{p}_2 + \mathbf{p}_3 + \dots + \mathbf{p}_N = 0$ in 3-dimensional momentum space. Thus, the joint N -particle probability distribution can be presented as [54, 55] :

$$f(\mathbf{p}_1, \mathbf{p}_2, \mathbf{p}_3, \dots, \mathbf{p}_N) = \frac{1}{A} \delta^3(\mathbf{p}_1 + \mathbf{p}_2 + \mathbf{p}_3 + \dots + \mathbf{p}_N) F(\mathbf{p}_1)F(\mathbf{p}_2)F(\mathbf{p}_3)\dots F(\mathbf{p}_N), \quad (4)$$

where A is an over-all normalization constant, $F(\mathbf{p})$ is the single-particle ‘unnormalized’ probability distribution function, and $\delta^3(\mathbf{p}_1 + \mathbf{p}_2 + \mathbf{p}_3 + \dots + \mathbf{p}_N)$ is for the global momentum conservation (GMC) constraint¹. Now the 2-particle joint distribution from the above equation can be obtained by integrating over all $N - 2$ momenta as follows:

¹ If we only consider of transverse momentum conservation, \mathbf{p} will be reduced to \mathbf{p}_T .

$$f(\mathbf{p}_1, \mathbf{p}_2) = \frac{1}{A} \left(\prod_{j=1}^2 F(\mathbf{p}_j) \right) \times \int \delta^3(\mathbf{p}_1 + \mathbf{p}_2 + \mathbf{p}_3 + \dots + \mathbf{p}_N) \prod_{j=3}^N \left[F(\mathbf{p}_j) d\mathbf{p}_j \right]. \quad (5)$$

Note that in the absence of GMC constraint, $F(\mathbf{p}) = f(\mathbf{p})$ and the joint probability distribution function simply factorizes to the product of two single-particle distribution functions.

For large N , we approximate the 2-particle joint probability distribution (or 2-particle cumulant) [54] as:

$$f(\mathbf{p}_1, \mathbf{p}_2) = F(\mathbf{p}_1)F(\mathbf{p}_2) \exp \left[-\frac{p_{1,x}p_{2,x}}{N\langle p_x^2 \rangle_F} - \frac{p_{1,y}p_{2,y}}{N\langle p_y^2 \rangle_F} - \frac{p_{1,z}p_{2,z}}{N\langle p_z^2 \rangle_F} \right], \quad (6)$$

where, x -, y - and z - axes are three principal axes that diagonalize the tensor $\langle \mathbf{p} \otimes \mathbf{p} \rangle$. The z -axis, conventionally, denotes the beam axis, whereas, x -axis represents the direction of impact parameter and y -axis lies perpendicular to the x -axis and z -axis. The quantity $\langle \dots \rangle_F$ in the above equation denotes the average obtained from full phase space integration as follows :

$$\langle O(\mathbf{p}) \rangle_F = \frac{\int_F O(\mathbf{p}) F(\mathbf{p}) d^3 \mathbf{p}}{\int_F F(\mathbf{p}) d^3 \mathbf{p}}. \quad (7)$$

In the Cartesian coordinate system, the 3-momentum (\mathbf{p}) of a particle can be written as :

$$\mathbf{p} = \begin{pmatrix} p_x = p_T \cos \phi \\ p_y = p_T \sin \phi \\ p_z = \sqrt{p_T^2 + m^2} \sinh y = p_T \sinh \eta \end{pmatrix}, \quad (8)$$

where, m , p_T , y ($= \frac{1}{2} \ln \frac{E+p_z}{E-p_z}$), η ($= \frac{1}{2} \ln \frac{p+p_z}{p-p_z}$) and ϕ are the mass, transverse momentum, rapidity, pseudorapidity, and momentum azimuthal angle of the particle, respectively.

The n th harmonic of two-particle azimuthal cumulant, i.e., $c_n\{2\} = \langle e^{in(\phi_1 - \phi_2)} \rangle$, can be obtained by performing the azimuthal integration of the two particle joint probability distribution as follows :

$$\begin{aligned} c_n\{2\} |_{\eta_1, p_{1,T}; \eta_2, p_{2,T}} &= \langle e^{in(\phi_1 - \phi_2)} \rangle \\ &= \frac{\int_0^{2\pi} \int_0^{2\pi} f(\mathbf{p}_1, \mathbf{p}_2) e^{in(\phi_1 - \phi_2)} d\phi_1 d\phi_2}{\int_0^{2\pi} \int_0^{2\pi} f(\mathbf{p}_1, \mathbf{p}_2) d\phi_1 d\phi_2}. \end{aligned} \quad (9)$$

B. Two-particle azimuthal cumulant from GMC + hydro-like flow

For hydro-like flow, we can approximate the single particle distribution at any pseudorapidity η as follows :

$$F(\mathbf{p}) = \frac{g(p, \eta)}{2\pi} \left[1 + \sum_n 2v_n(p, \eta) \cos[n(\phi - \psi_n(\eta))] \right], \quad (10)$$

where the $v_n(p, \eta)$ and $\psi_n(\eta)$ are the n -th order the differential flow parameter and the n -th event-plane angle at pseudorapidity η , respectively. Note that we represent p_T as p for simplicity. Next we will calculate the 2nd and 3rd order harmonics of the two-particle cumulants in the presence of hydro-like flow and GMC using Eq. (10) and Eq. (6).

Taking only the elliptic flow and expanding the Eq. (6) up to the second order ($1/N^2$), we get the following result

for the two-subevent $c_2\{2\}^2$:

$$\begin{aligned}
c_2\{2\} &= \langle e^{i2(\phi_1 - \phi_2)} \rangle_{\eta_1, p_1; \eta_2, p_2}^{\text{GMC+Flow}} \approx v_2(p_1, \eta_1) v_2(p_2, \eta_2) \cos[2(\psi_2(\eta_1) - \psi_2(\eta_2))] \\
&\quad - \frac{p_1 \sinh(\eta_1) p_2 \sinh(\eta_2) v_2(p_1, \eta_1) v_2(p_2, \eta_2) \cos[2(\psi_2(\eta_1) - \psi_2(\eta_2))]}{N \langle p_z^2 \rangle_F} \\
&\quad + \frac{p_1^2 \sinh^2(\eta_1) p_2^2 \sinh^2(\eta_2) v_2(p_1, \eta_1) v_2(p_2, \eta_2) \cos[2(\psi_2(\eta_1) - \psi_2(\eta_2))]}{2N^2 \langle p_z^2 \rangle_F^2} \\
&\quad + \frac{p_1^2 p_2^2 v_2(p_1, \eta_1) v_2(p_2, \eta_2) \cos[2(\psi_2(\eta_1) - 2\psi_2(\eta_2))]}{N^2 \langle p_T^2 \rangle_F^2} + \frac{p_1^2 p_2^2}{2N^2 \langle p_T^2 \rangle_F^2} \quad (11)
\end{aligned}$$

where we assume that $\langle p_x^2 \rangle_F \approx \langle p_y^2 \rangle_F \approx \langle p_T^2 \rangle_F / 2$. Similarly, after taking the momentum anisotropy flow up to third order harmonic and expanding the Eq. (6) up to the third power $1/N^3$, we can obtain the following result for the two-subevent $c_3\{2\}$:

$$\begin{aligned}
c_3\{2\} &= \langle e^{i3(\phi_1 - \phi_2)} \rangle_{\eta_1, p_1; \eta_2, p_2}^{\text{GMC+Flow}} \approx v_3(p_1, \eta_1) v_3(p_2, \eta_2) \cos[3(\psi_3(\eta_1) - \psi_3(\eta_2))] \\
&\quad - \frac{p_1 p_2 v_2(p_1, \eta_1) v_2(p_2, \eta_2) \cos[2(\psi_2(\eta_1) - \psi_2(\eta_2))]}{N \langle p_T^2 \rangle_F} \\
&\quad - \frac{p_1 \sinh(\eta_1) p_2 \sinh(\eta_2) v_3(p_1, \eta_1) v_3(p_2, \eta_2) \cos[3(\psi_3(\eta_1) - \psi_3(\eta_2))]}{N \langle p_z^2 \rangle_F} \\
&\quad + \frac{p_1^2 p_2^2 v_3(p_1, \eta_1) v_3(p_2, \eta_2) \cos[3(\psi_3(\eta_1) - \psi_3(\eta_2))]}{N^2 \langle p_T^2 \rangle_F^2} \\
&\quad + \frac{p_1^2 \sinh(\eta_1) p_2^2 \sinh(\eta_2) v_2(p_1, \eta_1) v_2(p_2, \eta_2) \cos[2(\psi_2(\eta_1) - \psi_2(\eta_2))]}{N^2 \langle p_T^2 \rangle_F \langle p_z^2 \rangle_F} \\
&\quad + \frac{p_1^2 \sinh^2(\eta_1) p_2^2 \sinh^2(\eta_2) v_3(p_1, \eta_1) v_3(p_2, \eta_2) \cos[3(\psi_3(\eta_1) - \psi_3(\eta_2))]}{2N^2 \langle p_z^2 \rangle_F^2} \\
&\quad - \frac{p_1^3 p_2^3 v_2(p_1, \eta_1) v_2(p_2, \eta_2) \cos[2(\psi_2(\eta_1) - \psi_2(\eta_2))]}{2N^3 \langle p_T^2 \rangle_F^3} \\
&\quad - \frac{p_1^3 \sinh(\eta_1) p_2^3 \sinh(\eta_2) v_3(p_1, \eta_1) v_3(p_2, \eta_2) \cos[3(\psi_3(\eta_1) - \psi_3(\eta_2))]}{N^3 \langle p_T^2 \rangle_F^2 \langle p_z^2 \rangle_F} \\
&\quad - \frac{p_1^3 \sinh^2(\eta_1) p_2^3 \sinh^2(\eta_2) v_2(p_1, \eta_1) v_2(p_2, \eta_2) \cos[2(\psi_2(\eta_1) - \psi_2(\eta_2))]}{2N^3 \langle p_T^2 \rangle_F \langle p_z^2 \rangle_F^2} \\
&\quad - \frac{p_1^3 \sinh^3(\eta_1) p_2^3 \sinh^3(\eta_2) v_3(p_1, \eta_1) v_3(p_2, \eta_2) \cos[3(\psi_3(\eta_1) - \psi_3(\eta_2))]}{6N^3 \langle p_z^2 \rangle_F^3} \\
&\quad - \frac{p_1^3 p_2^3}{6N^3 \langle p_T^2 \rangle_F^3}. \quad (12)
\end{aligned}$$

In both Eq. (11) and Eq. (12), we can see a pure flow-contributed term $[v_n(p_1, \eta_1) v_n(p_2, \eta_2) \cos[n(\psi_n(\eta_1) - \psi_n(\eta_2))]]$ and a flow-independent term $[(-1)^n \frac{p_1^n p_2^n}{n! N^n \langle p_T^2 \rangle_F^n}]$ which was found to be due to transverse momentum conservation [56]. In fact, the first one arises from the ‘‘indirect’’ part of the joint probability distribution, whereas, the second term comes from the ‘‘direct’’ part of the joint probability distribution. The rest of the terms are of the order of $\mathcal{O}(1/N)$, $\mathcal{O}(1/N^2)$ or higher power, which arise from the interplay between the GMC and hydro-like flow.

To estimate the first order correction in the two-particle correlation under the influence of GMC, we drop all the

² Note that evaluating Eq. (9), the denominator is considered as $4\pi^2$ only, as the other terms are suppressed by the higher power of $1/N$

terms with $\mathcal{O}(1/N^2)$ and higher powers³. Consequently, Eq. (11) and Eq. (12) appear simpler as follows:

$$c_2\{2\} = \langle e^{i2(\phi_1 - \phi_2)} \rangle_{\eta_1, p_1; \eta_2, p_2}^{\text{GMC+Flow}} \approx v_2(p_1, \eta_1) v_2(p_2, \eta_2) \cos[2(\psi_2(\eta_1) - \psi_2(\eta_2))] - \frac{p_1 \sinh(\eta_1) p_2 \sinh(\eta_2) v_2(p_1, \eta_1) v_2(p_2, \eta_2) \cos[2(\psi_2(\eta_1) - \psi_2(\eta_2))]}{N \langle p_z^2 \rangle_F}, \quad (13)$$

$$c_3\{2\} = \langle e^{i3(\phi_1 - \phi_2)} \rangle_{\eta_1, p_1; \eta_2, p_2}^{\text{GMC+Flow}} \approx v_3(p_1, \eta_1) v_3(p_2, \eta_2) \cos[3(\psi_3(\eta_1) - \psi_3(\eta_2))] - \frac{p_1 p_2 v_2(p_1, \eta_1) v_2(p_2, \eta_2) \cos[2(\psi_2(\eta_1) - \psi_2(\eta_2))]}{N \langle p_T^2 \rangle_F} - \frac{p_1 \sinh(\eta_1) p_2 \sinh(\eta_2) v_3(p_1, \eta_1) v_3(p_2, \eta_2) \cos[3(\psi_3(\eta_1) - \psi_3(\eta_2))]}{N \langle p_z^2 \rangle_F}. \quad (14)$$

Form the above two equations, we can see that the two-particle azimuthal cumulants can be modified by the constraint of the GMC. We will later show that the effect from the GMC further leads a modification of longitudinal decorrelation of harmonic flow.

III. LONGITUDINAL FLOW DECORRELATION FROM GMC

A. Definition of longitudinal flow decorrelation r_n

The longitudinal decorrelation of harmonic flow measures the decorrelation effects between two symmetric pseudorapidity bins (i.e., $-\eta$ and η) along the longitudinal direction by comparing the correlations between each of them and a reference pseudorapidity bin η_r (which is usually chosen a large value to avoid non-flow contribution). The observable is defined as :

$$r_n(\eta, \eta_r) = \frac{\langle \mathbf{Q}_n(-\eta) \mathbf{Q}_n^*(\eta_r) \rangle}{\langle \mathbf{Q}_n(\eta) \mathbf{Q}_n^*(\eta_r) \rangle}, \quad (15)$$

where the $\mathbf{Q}_n(\eta)$ vector quantifies the n -th order harmonic flow in a collision event,

$$\mathbf{Q}_n(\eta) = \frac{1}{M} \sum_{i=1}^M e^{in\phi_i}, \quad (16)$$

where M represents the number of particles in the corresponding pseudorapidity η bin. The longitudinal flow decorrelation coefficient r_n can further be expressed in terms of two-particle correlation :

$$r_n(\eta, \eta_r) = \frac{\langle e^{in(\phi_1(-\eta) - \phi_2(\eta_r))} \rangle}{\langle e^{in(\phi_1(\eta) - \phi_2(\eta_r))} \rangle}. \quad (17)$$

If there is only ‘‘indirect’’ correlation term but no ‘‘direct’’ correlation term present in the the 2-particle correlation in Eq. (1), r_n can be expressed as:

$$r_n(\eta, \eta_r)|_{-\eta; \eta; \eta_r}^{\text{Flow}} = \frac{\langle v_n(-\eta) v_n(\eta_r) \cos(n(\psi_n(-\eta) - \psi_n(\eta_r))) \rangle}{\langle v_n(\eta) v_n(\eta_r) \cos(n(\psi_n(\eta) - \psi_n(\eta_r))) \rangle}, \quad (18)$$

which reflects a normal form of longitudinal flow decorrelation due to hydro-like flow.

B. Longitudinal flow decorrelation r_n from GMC + hydro-like flow

In the presence of both ‘‘indirect’’ and ‘‘direct’’ correlations like both hydro-like flow and GMC, the r_n for $n = 2, 3$ can be evaluated by inserting the Eq. (13) and Eq. (14) into the following relation :

$$r_n(\eta, \eta_r)|_{-\eta, p_1; \eta, p_2; \eta_r, p_3}^{\text{GMC+Flow}} = \frac{\langle e^{in(\phi_1 - \phi_2)} \rangle_{-\eta, p_1; \eta_r, p_3}^{\text{GMC+Flow}}}{\langle e^{in(\phi_1 - \phi_2)} \rangle_{\eta, p_2; \eta_r, p_3}^{\text{GMC+Flow}}}. \quad (19)$$

³ We have checked that these higher orders of terms do not significantly change our results below.

The above equation expresses a momentum-dependent (or differential) form of r_n . However, such a variable can mimic the actual momentum-integrated observable (for example the transverse momentum window is considered to be $0.3 \text{ GeV} < p < 3 \text{ GeV}$ for the Pb+Pb collisions at the LHC experiment), if a relevant mean p is chosen. We consider the transverse momenta of the particles at the forward, backward (i.e., $\pm \eta$) and at the reference pseudorapidity (η_r) to be equal to each other (i.e., $p_1 \approx p_2 \approx p_3 = p$, for $i = 1, 2$ and 3) and subsequently by inserting Eq. (13) into the Eq. (19), we can obtain the second order longitudinal flow decorrelation coefficient [i.e., $r_2(\eta, \eta_r)$]:

$$r_2(\eta, \eta_r) \Big|_{-\eta, p; \eta, p; \eta_r, p}^{\text{GMC+Flow}} = r_2(\eta, \eta_r) \Big|_{-\eta, p; \eta, p; \eta_r, p}^{\text{Flow}} \times R_2$$

$$\text{where, } R_2 \approx \left[\frac{p^2 \sinh(-\eta) \sinh(\eta_r) - N \langle p_z^2 \rangle_F}{p^2 \sinh(\eta) \sinh(\eta_r) - N \langle p_z^2 \rangle_F} \right]. \quad (20)$$

As we can see from the above equation, the modification term for r_2 (denoted by R_2 here) appears due to the effects of GMC, which depends on the longitudinal momentum distribution of particles and the total number of particles in the collision system. If the value of R_2 is one, it indicates no change in the decorrelation parameter value. If R_2 is greater than one, it indicates that the longitudinal decorrelation is weakened due to the presence of the GMC. However, a fractional value of R_2 indicate a stronger decorrelation in the presence of the GMC.

Similarly, an approximated expression for longitudinal decorrelation parameter r_3 using Eq. (14) appears as:

$$r_3(\eta, \eta_r) \Big|_{-\eta, p; \eta, p; \eta_r, p}^{\text{GMC+Flow}} = r_3(\eta, \eta_r) \Big|_{-\eta, p; \eta, p; \eta_r, p}^{\text{Flow}} \times R_3$$

where,

$$R_3 \approx \frac{D}{C} \left[\frac{p^2 \langle p_z^2 \rangle_F v_2(p, -\eta) v_2(p, \eta_r) v_3(p, \eta) A - \langle p_T^2 \rangle_F v_3(p, \eta) v_3(p, -\eta) v_3(p, \eta_r) C (N \langle p_z^2 \rangle_F + p^2 \sinh(\eta) \sinh(\eta_r))}{p^2 \langle p_z^2 \rangle_F v_2(p, \eta) v_2(p, \eta_r) v_3(p, -\eta) B - \langle p_T^2 \rangle_F v_3(p, -\eta) v_3(p, \eta) v_3(p, \eta_r) D (N \langle p_z^2 \rangle_F - p^2 \sinh(\eta) \sinh(\eta_r))} \right] \quad (21)$$

where,

$$A = \cos[2(\psi_2(-\eta) - \psi_2(\eta_r))], B = \cos[2(\psi_2(\eta) - \psi_2(\eta_r))], C = \cos[3(\psi_3(-\eta) - \psi_3(\eta_r))], \text{ and } D = \cos[3(\psi_3(\eta) - \psi_3(\eta_r))]$$

In the next section, we will discuss how to obtain the estimates of $\langle p_z^2 \rangle_F$ and N from a longitudinally accelerating perfect fluid system in order to calculate the effects of GMC on the longitudinal flow decorrelation coefficients.

IV. ESTIMATE OF KEY PARAMETERS ($\langle p_z^2 \rangle_F$ AND N_F) FROM IDEAL HYDRODYNAMICS

The production and anisotropic flow of charged hadrons are successfully described in relativistic hydrodynamic framework. Both viscous and ideal hydrodynamic models have been found to provide satisfactory description of the hadronic yields for various collision systems at the energies available at the RHIC and LHC. For the present study, we aim to find the estimates of $\langle p_z^2 \rangle_F$ and N from a longitudinally expanding fireball. We follow Ref. [59] to obtain the pseudorapidity distribution of charged hadrons in a longitudinally accelerating perfect fluid system in which the net baryon number and energy-momentum tensor follow the conservation laws. An approximate parametric relation for the rapidity distribution of charged hadrons in a perfect fluid system is as follows:

$$\frac{dN_{\text{ch}}}{dy} \approx N_0 \cosh^{-\frac{1}{2}\alpha(\lambda)-1} \left(\frac{y}{\alpha(\lambda)} \right) \exp \left(- \frac{m}{T_f} \cosh^{\alpha(\lambda)} \left(\frac{y}{\alpha(\lambda)} \right) \right), \quad (22)$$

where $\alpha(\lambda) = \frac{2\lambda-1}{\lambda-1}$, and N_0, T_f , and λ are three fit parameters. To obtain the pseudorapidity distribution of charged hadrons with average mass \bar{m} , we use the following relation :

$$\frac{dN_{\text{ch}}}{d\eta} \approx \frac{\cosh \eta}{\sqrt{D^2 + \cosh^2 \eta}} \frac{dN_{\text{ch}}}{dy} \Big|_{y=y(\eta)}, \quad (23)$$

where the parameter $D = \bar{m} / \left[\frac{T_{\text{eff}}}{1 + \frac{\sigma^2}{2}(y - y_{\text{mid}})^2} \right]$ determines the dip of the pseudorapidity distribution at the mid-rapidity. The other two fit parameters are T_{eff} and σ . The significance of these used parameters are listed as follows,

- N_0 is a normalization constant that fixes the particle density at mid-rapidity.
- T_f corresponds to the freeze-out temperature.

- λ determines the longitudinal acceleration of the fluid.
- The effective temperature T_{eff} corresponds to the inverse slope parameter of $m_T - m$ spectra at the mid-rapidity.
- σ parameterizes the effective temperature gradient.

The pseudorapidity distribution of all particles (i.e., charged+neutral = $\frac{dN}{d\eta}$) at any pseudorapidity bin η can be further approximated as, $\frac{dN}{d\eta} \approx 1.5 \frac{dN_{\text{ch}}}{d\eta}$. Finally, the average of the variable p_z^2 for all particles, $\langle p_z^2 \rangle_{\Gamma}$, over a phase space region $\Gamma \in \{-\eta, \eta\}$ (in terms of pseudorapidity range) is obtained by performing the following integral:

$$\langle p_z^2 \rangle_{\Gamma} = \frac{\int_{\Gamma} p_z^2 \frac{dN}{d\eta} d\eta}{\int_{\Gamma} \frac{dN}{d\eta} d\eta}. \quad (24)$$

The total number of particles N within the phase-space region $\Gamma \in \{-\eta, \eta\}$ can be calculated by,

$$N_{\Gamma} = \int_{\Gamma} \frac{dN}{d\eta} d\eta. \quad (25)$$

V. RESULTS AND DISCUSSION

A. $\langle p_z^2 \rangle_{\Gamma}$ and N_{Γ} for Pb+Pb collisions at 2.76A TeV at the LHC

In section III, we have shown that the longitudinal momentum distribution of particles plays a key role in determining the effects of GMC on the longitudinal flow decorrelation. The question arises, how can one determine phase space volume for the global momentum conservation in relativistic heavy-ion collisions. Ideally, the full phase-space volume should be considered. In reality, there might be some particles residing at the high η region of the pseudorapidity distribution (i.e., large longitudinal momentum) originated from the spectators far away from the collision zone. Such particles should not be taken into consideration as they are not the products of the collision zone. Therefore, we only consider a finite phase space region for global momentum conservation to mimic the real case.

We use the relativistic hydrodynamical framework described in section IV to fit the experimental data of charged

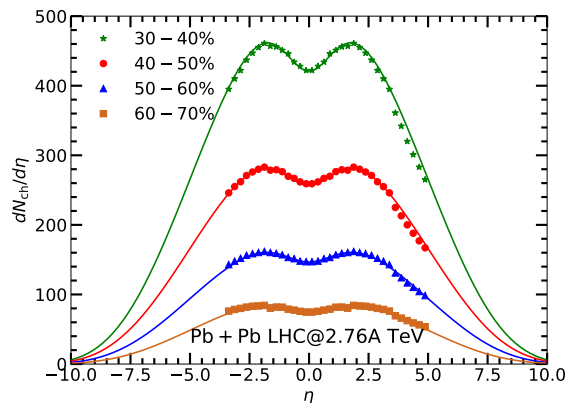


FIG. 1: (Color online) Charged particle pseudorapidity density for 30 – 40%, 40 – 50%, 50 – 60% and 60 – 70% centrality bins in Pb+Pb collisions at $\sqrt{s_{NN}} = 2.76$ TeV, where the charged particle pseudorapidity distributions for four centrality bins are fitted with the parameters presented in the TABLE I.

particle pseudorapidity distributions for four different centrality bins (i.e., 30 – 40%, 40 – 50%, 50 – 60% and 60 – 70%) of Pb+Pb collisions at 2.76A TeV at ALICE. Consequently, we evaluate various needed quantities to determine the effects of the GMC on longitudinal decorrelation parameters r_n .

We use the fit parameters shown in TABLE I (obtained from Ref. [59]) to reproduce the pseudorapidity distribution of charged hadrons from Pb+Pb collisions at 2.76A TeV. The average mass (\bar{m}) of all charged hadrons is taken as 0.24 GeV, and the value of freeze-out temperature (T_f) is taken as 0.09 GeV. The central pseudorapidity density

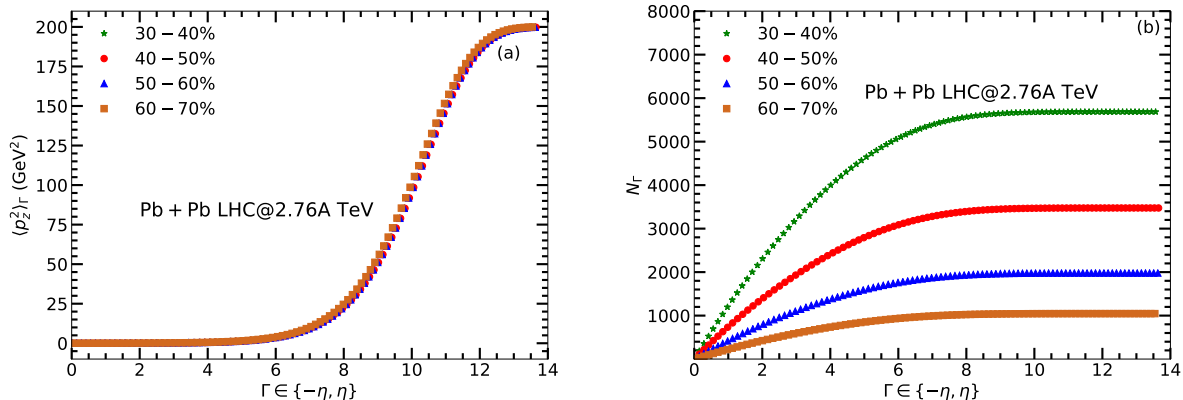


FIG. 2: (Color online) (a) $\langle p_z^2 \rangle_\Gamma$ and (b) N_Γ as a function of phase space region $\Gamma \in \{-\eta, \eta\}$ for 30 – 40%, 40 – 50%, 50 – 60% and 60 – 70% centrality bins in Pb+Pb collisions at $\sqrt{s_{NN}} = 2.76$ TeV.

$(dN_{ch}/d\eta)|_{\eta=0}$ for 30 – 40%, 40 – 50%, 50 – 60% and 60 – 70% centrality bins of Pb+Pb collisions at 2.76A TeV are taken as 422.0, 259.1, 147.1, and 74.7, respectively. As shown in Fig. 1, the parameter set presented in TABLE-I is able to describe the pseudorapidity distributions of charged hadrons for all four centrality bins satisfactorily. We further approximate the total number of particles as 1.5 times the charged hadron multiplicity.

TABLE I: Fit parameters in Fig. 1 using Eq. (22) for Pb+Pb collisions at 2.76A TeV [59], where the auxiliary values of $T_f = 0.09$ GeV and $\bar{m} = 0.24$ GeV have been utilized.

| | $\left. \frac{dN_{ch}}{d\eta} \right _{\eta=0}$ | λ | σ | $T_{eff}(\text{GeV})$ |
|----------|---|-----------|----------|-----------------------|
| 30 – 40% | 422.0 | 1.04 | 0.88 | 0.27 |
| 40 – 50% | 259.1 | 1.04 | 0.92 | 0.27 |
| 50 – 60% | 147.1 | 1.04 | 0.91 | 0.27 |
| 60 – 70% | 74.7 | 1.04 | 0.87 | 0.27 |

In Fig. 2, we show the $\langle p_z^2 \rangle_\Gamma$ and $\langle N \rangle_\Gamma$ of all particles as a function of phase-space interval Γ (i.e., pseudorapidity range) for Pb+Pb collisions at 2.76A TeV at the LHC. The $\langle p_z^2 \rangle_\Gamma$ over a phase-space interval $\Gamma \in \{-\eta, \eta\}$ is computed by using Eq. (25). In Fig. 2(a), the $\langle p_z^2 \rangle_\Gamma$ as function of Γ for four centrality 30 – 40%, 40 – 50%, 50 – 60% and 60 – 70% in Pb+Pb collisions at 2.76A TeV are presented. We find that the value of $\langle p_z^2 \rangle_\Gamma$ increases slowly upto $\Gamma \in \{-6, 6\}$, then it starts to increase exponentially and finally saturates above $\Gamma \in \{-12, 12\}$. The values of $\langle p_z^2 \rangle_\Gamma$ for all four centrality bins are found to be close to each other. In Fig. 2(b), the $\langle N \rangle_\Gamma$ as a function of Γ for the above centrality bins are shown. As we take into account a larger phase-space region, the average number of particles inside it starts to increase sharply and finally saturates above the pseudorapidity window $\Gamma \in \{-8, 8\}$, when it reaches the beam rapidity. We also see that the average number of particles for the 30 – 40% centrality bin is almost 1.7, 3, and 6 times as large as 40 – 50%, 50 – 60%, and 60 – 70% centrality bins, respectively.

B. R_2 and R_3 for Pb+Pb collisions at 2.76A TeV at the LHC

With the above information about $\langle N \rangle_\Gamma$ and $\langle p_z^2 \rangle_\Gamma$, we present the behaviour of modification factor R_2 as function of η for Pb+Pb collisions at 2.76A TeV in Fig. 3. In Fig. 3(a), we show the η dependence of R_2 for 60-70% centrality bin for three selected phase volumes (i.e., $\Gamma \in \{-\eta, \eta\}$). We see that R_2 increases with η due to the constraint of the GMC effect. We observe that the effect of GMC on R_2 tends to increase if the phase space volume with the GMC constraint gets smaller. Among three chosen phase space regions, i.e. $\Gamma \in \{-8, 8\}$, $\{-7, 7\}$, and $\{-6, 6\}$, the effects on R_2 are found to be largest for the $\Gamma \in \{-6, 6\}$. These features can be understood according to the form of modification factor R_2 shown in Eq. (20). Note that the recent ALICE result supports that baryon number follows a global baryon number conservation in Pb+Pb collisions at the LHC [60].

In Fig. 3(b), we show R_2 as a function of η for various centrality bins for Pb+Pb collisions at 2.76A TeV, where

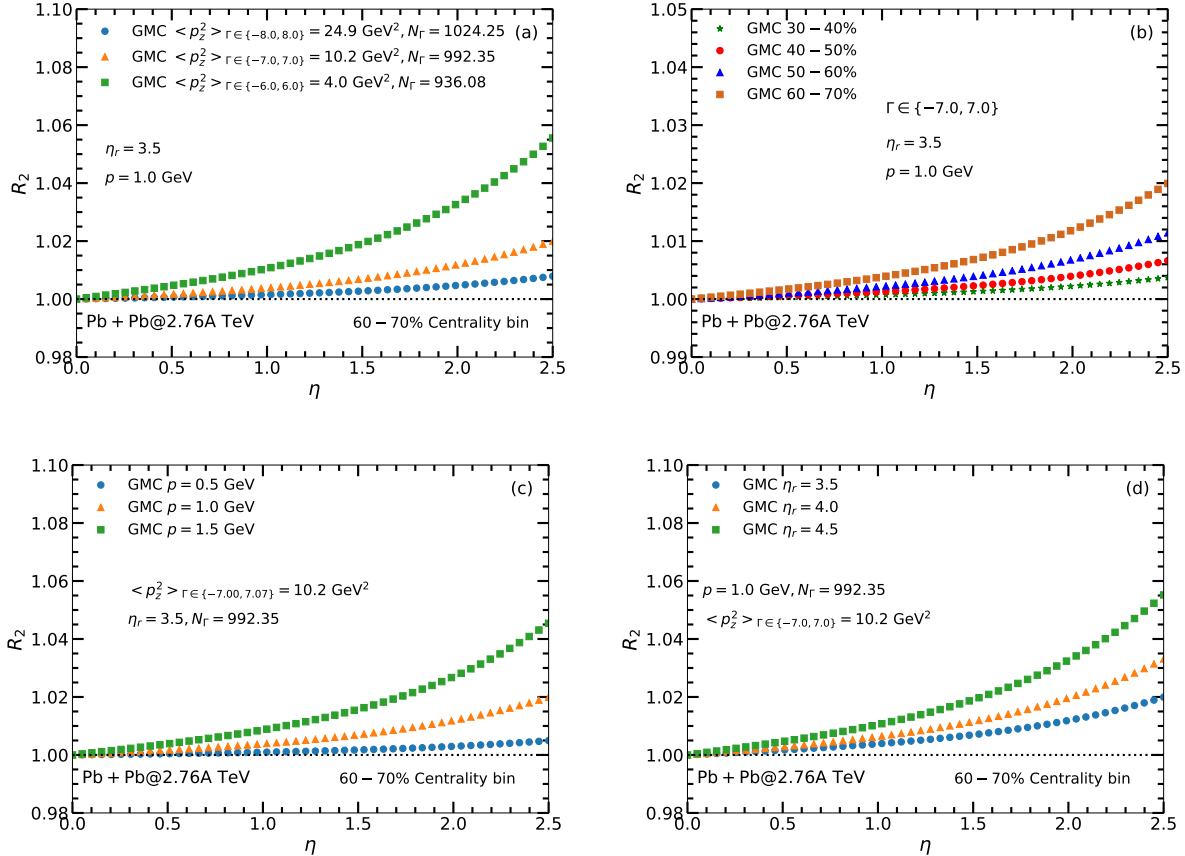


FIG. 3: (Color online) The modification factor of longitudinal decorrelation R_2 as a function of η for (a) different phase-space volumes with GMC constraint, (b) different centrality bins, (c) different momenta and, (d) different reference pseudorapidities in Pb+Pb collisions at $\sqrt{s_{NN}} = 2.76$ TeV.

we assume that the GMC constraint is valid within $\Gamma \in \{-7, 7\}$ for all the centrality bins. We see that the GMC has more impact on the peripheral collisions than the central collisions. In Fig. 3(c), we show the η dependence of R_2 for the different transverse momenta p of particles for the centrality bin of 60-70% in Pb+Pb collisions at 2.76A TeV, where we choose $p_1 = p_2 = p_3 = p$. As the value of transverse momentum increases, the effect of GMC is found to increase. For $p = 1.5$ GeV, the GMC effect are found to be the largest compared to the same obtained from the smaller momentum values. It should be pointed out that so far we have computed the momentum-dependent observable with fixed momentum values; however, in experiments, the longitudinal decorrelation was measured for all charged particles within the momentum range, e.g. $0.3 \text{ GeV} < p < 3.0 \text{ GeV}$. We expect that the behavior of the momentum-integrated decorrelation under the influence of GMC will be similar to that shown here. (see Appendix-I).

In Fig. 3(d), we show the η dependence of R_2 for different reference pseudorapidity (η_r) for the centrality bin of 60-70% in Pb+Pb collisions at 2.76A TeV. We find that the effect of GMC increases as η_r gets further away, resulting in a smaller longitudinal decorrelation. In fact, a similar reference pseudorapidity dependence of $r_n(\eta, \eta_r)$ has been observed for Pb+Pb and p+Pb collisions at the LHC, where the decorrelation effect has been shown to be weaker for a larger reference pseudorapidity bin [38].

In Fig. 4, we further elaborate the reference pseudorapidity dependence of the GMC-induced results by comparing the ratio of two longitudinal decorrelation coefficients at separate reference pseudorapidity bins [$r_2(\eta, \eta_{rA})/r_2(\eta, \eta_{rB})$] with the CMS data [38]. Here we compute the ratio of r_2 with different η_r for different centrality bins in Pb+Pb collisions, and compare our findings with the results obtained from the experimental measurements. In this way, we hope to cancel the flow contribution to show a clearer effect of the GMC. Surprisingly, by invoking the effect of GMC, we can describe the reference pseudorapidity dependence of the data for peripheral collisions. In Fig. 4 (a), (b) and (c) we compare the experimental $r_2(\eta, \eta_r = 3.5)/r_2(\eta, \eta_r = 4.7)$ ratio with our theoretical results for 30 – 40%, 40 – 50% and 50 – 60% centrality bins in Pb+Pb collisions at 2.76A TeV, respectively. We find that our results with momentum $p \sim 1.0 \pm 0.1 \text{ GeV}$ can satisfactorily describe the data for all three centrality bins. We also find that

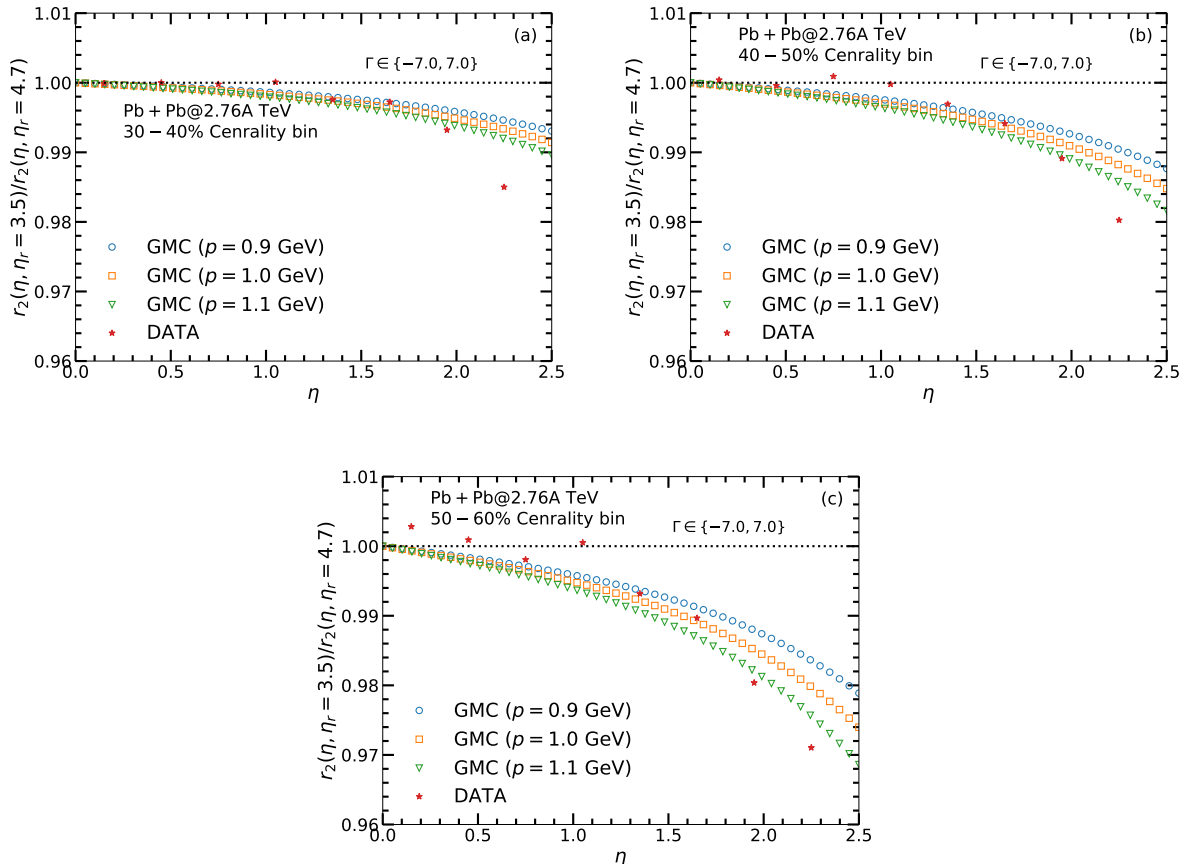


FIG. 4: (Color online) The ratio of $r_2(\eta_1, \eta_r = 3.5)/r_2(\eta_1, \eta_r = 4.7)$ as a function of η for (a) 30 – 40%, (b) 40 – 50% and (c) 50 – 60% in Pb+Pb collisions at $\sqrt{s_{NN}} = 2.76$ TeV.

such reference pseudorapidity dependence is even enhanced if the GMC is considered for a smaller region of phase space.

The pseudorapidity dependence of $r_2(\eta, \eta_{rA})/r_2(\eta, \eta_{rB})$ ratio is further explored for Au+Au collisions at the RHIC energy in Fig. 5. We simultaneously compare the ratios of $r_2(\eta, \eta_r = 2.35)/r_2(\eta, \eta_r = 3.4)$ for 30-40% and 40-50% centrality bins in Pb+Pb collisions at 2.76A TeV and Au+Au collisions at 0.2A TeV. We find that the ratio is more significantly affected in Au+Au collisions at the RHIC energy than that in Pb+Pb collisions at the LHC energy. Note that the two results for two centrality bins in Pb+Pb collisions at 2.76A TeV are almost overlapping and consistent with one for such η_r selection. We also see that the ratio is larger for more peripheral collisions at RHIC. We have noticed that the longitudinal decorrelation coefficient r_2 has been measured for several reference pseudorapidity bins in isobar collisions at 0.2A TeV and a similar pseudorapidity dependence of $r_2(\eta, \eta_{rA})/r_2(\eta, \eta_{rB})$ has been observed [42].

In addition, we follow Eq. (21) to explore the behavior of R_3 in Pb+Pb collisions at 2.76A TeV. We find that R_3 behaves similarly as R_2 because the dominant contribution comes the terms which consist v_3 's only (if with the v_3 only terms, $R_3 \equiv R_2$). We further check the contribution of v_2 terms in Eq. (21). By assuming, $\langle \cos[n(\psi_a - \psi_r)] \rangle \approx e^{-F_n |\eta_a - \eta_r|}$ (for $n=2,3$) and the values of F_2 , F_3 , v_2 and v_3 to be 0.02, 0.04, 0.05 and 0.025, respectively, we find that the inclusion of v_2 -involving terms introduces a decrement in R_3 [i.e. $\Delta R_3/(R_3 - 1) \times 100\%$] by 10 – 15%.

VI. SUMMARY

In summary, we explore the effect of the global momentum conservation on the longitudinal flow decorrelation coefficients. We first present the analytic forms of two particle azimuthal cumulants and the decorrelation coefficients, subsequently, we explore the role of the GMC on the correction of the longitudinal flow decorrelation in Pb+Pb collisions at the LHC energy and Au+Au collisions at the RHIC energy. The modification factors R_2 and R_3 of the second and third order longitudinal flow decorrelation coefficients will weaken the longitudinal flow decorrelation due

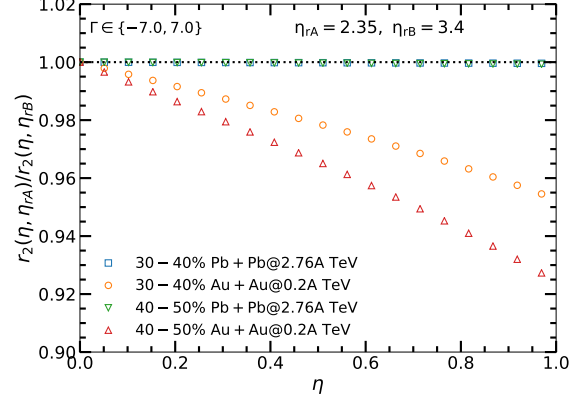


FIG. 5: (Color online) The ratio of $r_2(\eta_1, \eta_r = 2.35)$ over $r_2(\eta_1, \eta_r = 3.4)$ as a function of η for 30 – 40% and 40 – 50% Pb+Pb collisions at 2.76A TeV and Au+Au collisions at 0.2A TeV.

to the presence of GMC. We find that the modification factor is sensitive to the total number of involved particles (N), the average longitudinal momentum $\langle p_z^2 \rangle_F$ and the reference pseudorapidity (η_r). Our results of $r_2(\eta, \eta_{rA})/r_2(\eta, \eta_{rB})$ ratios are consistent with the experimental measurements. We also predict that the modification effect is stronger for RHIC energy than that for LHC energy. Our findings suggest that we should consider the effect of GMC constraint in the study of longitudinal flow decorrelation in relativistic heavy-ion collisions.

Acknowledgments

This work is supported by the National Natural Science Foundation of China under Grants No. 12150410303, No.12147101, No. 11890714, No. 11835002, No. 11961131011, No. 11421505, the Strategic Priority Research Program of Chinese Academy of Sciences under Grant No. XDB34030000, and the Guangdong Major Project of Basic and Applied Basic Research under Grant No. 2020B0301030008.

Appendix I

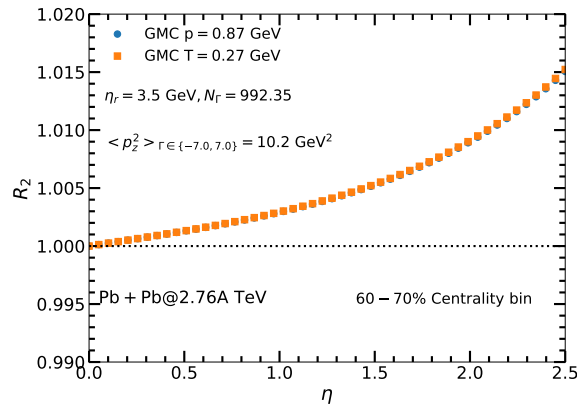


FIG. 6: (Color online) The modification factor R_2 corresponding to the integrated longitudinal decorrelation coefficient for 60 – 70% Pb+Pb collisions at 2.76A TeV at the LHC, in comparison with R_2 corresponding to $p \approx 0.87$ GeV.

In this section, we present the integrated longitudinal decorrelation coefficient, i.e., $r_2(\eta, \eta_r)$, under the influence of GMC. $F(\mathbf{p})$ is the single particle distribution function having a form as shown in Eq. (10). Considering A+A collision

system to be symmetric, we further assume the following forms of the pseudorapidity and momentum dependent function $g(p, \eta)$ and $v_2(p, \eta)$ [62]:

$$g(p, \eta) = \frac{1}{T^2} \exp\left(-\frac{p}{T}\right) h_1(\eta), \quad v_2(p, \eta) = p h_2(\eta) \quad (26)$$

where, $h_1(\eta)$ and $h_2(\eta)$ are two even functions of pseudorapidity. Now, introducing the above forms of the single and joint probability distribution functions into Eq. (17), and performing a momentum p integration over p_l to p_h , we finally obtain the integrated form of $r_2(\eta, \eta_r)$:

$$r_2(\eta, \eta_r)|^{\text{GMC+Flow}} = r_2(\eta, \eta_r)|^{\text{Flow}} \times R_2, \quad (27)$$

$$R_2 \approx \frac{N\langle p_z^2 \rangle_F(x(p_h, T)e^{p_l/T} - e^{p_h/T}x(p_l, T))^2 + \sinh(\eta) \sinh(\eta_r) (y(p_h, T)e^{p_l/T} - e^{p_h/T}y(p_l, T))^2}{N\langle p_z^2 \rangle_F(x(p_h, T)e^{p_l/T} - e^{p_h/T}x(p_l, T))^2 - \sinh(\eta) \sinh(\eta_r) (y(p_h, T)e^{p_l/T} - e^{p_h/T}y(p_l, T))^2}$$

where, $x(p, T) = p^2 + 2pT + 2T^2$ and $y(p, T) = p^3 + 3p^2T + 6pT^2 + 6T^3$

In Fig. 6, we show the η dependence of R_2 corresponding to the transverse momentum integrated longitudinal decorrelation coefficient for 60 – 70% Pb+Pb collisions at 2.76A TeV at the LHC. The integration limit has been chosen as $0.3 \text{ GeV} < p < 3.0 \text{ GeV}$ [38]. Subsequently, we compare our result with the differential R_2 obtained using Eq. (20) for the same collision system, and we observe that the result for $p \approx 0.87 \text{ GeV}$ agrees with the integrated longitudinal decorrelation coefficient. This further proves that the above results at a mean p value are reasonable to predict the behaviours of the integrated longitudinal decorrelation coefficients.

-
- [1] J. C. Collins and M. J. Perry, Phys. Rev. Lett. **34**, 1353 (1975).
 - [2] E. V. Shuryak, Phys. Rept. **61**, 71-158 (1980).
 - [3] A. Bzdak, S. Esumi, V. Koch, J. Liao, M. Stephanov and N. Xu, Phys. Rept. **853**, 1-87 (2020).
 - [4] X. Luo and N. Xu, Nucl. Sci. Tech. **28**, no.8, 112 (2017).
 - [5] S. S. Adler *et al.* [PHENIX], Phys. Rev. Lett. **91**, 182301 (2003).
 - [6] J. Adams *et al.* [STAR], Phys. Rev. Lett. **92**, 052302 (2004).
 - [7] J. Adams *et al.* [STAR], Phys. Rev. Lett. **92**, 062301 (2004) [erratum: Phys. Rev. Lett. **127**, no.6, 069901 (2021)].
 - [8] K. Aamodt *et al.* [ALICE], Phys. Rev. Lett. **105**, 252302 (2010).
 - [9] G. Aad *et al.* [ATLAS], Phys. Lett. B **707**, 330-348 (2012).
 - [10] J. Y. Ollitrault, Phys. Rev. D **46**, 229-245 (1992).
 - [11] D. H. Rischke, S. Bernard and J. A. Maruhn, Nucl. Phys. A **595**, 346-382 (1995).
 - [12] R. S. Bhalerao, Pramana **61**, 1021-1025 (2003).
 - [13] U. Heinz and R. Snellings, Ann. Rev. Nucl. Part. Sci. **63**, 123-151 (2013).
 - [14] C. Gale, S. Jeon and B. Schenke, Int. J. Mod. Phys. A **28**, 1340011 (2013).
 - [15] P. Huovinen, Int. J. Mod. Phys. E **22**, 1330029 (2013).
 - [16] H. Song, Y. Zhou and K. Gajdosova, Nucl. Sci. Tech. **28**, no.7, 99 (2017).
 - [17] C. Shen and L. Yan, Nucl. Sci. Tech. **31**, no.12, 122.
 - [18] G. Y. Qin, H. Petersen, S. A. Bass and B. Muller, Phys. Rev. C **82**, 064903 (2010).
 - [19] J. Noronha-Hostler, L. Yan, F. G. Gardim and J. Y. Ollitrault, Phys. Rev. C **93**, no.1, 014909 (2016).
 - [20] H. Holopainen, H. Niemi and K. J. Eskola, Phys. Rev. C **83**, 034901 (2011).
 - [21] H. Niemi, G. S. Denicol, H. Holopainen and P. Huovinen, Phys. Rev. C **87**, no.5, 054901 (2013).
 - [22] F. G. Gardim, F. Grassi, M. Luzum and J. Y. Ollitrault, Phys. Rev. C **85**, 024908 (2012).
 - [23] A. Bzdak, B. Schenke, P. Tribedy and R. Venugopalan, Phys. Rev. C **87**, no.6, 064906 (2013).
 - [24] B. H. Alver, C. Gombeaud, M. Luzum and J. Y. Ollitrault, Phys. Rev. C **82**, 034913(2010).
 - [25] V. Greco, M. Colonna, M. Di Toro and G. Ferini, Prog. Part. Nucl. Phys. **62**, 562 (2009).
 - [26] A. Jaiswal and V. Roy, Adv. High Energy Phys. **2016**, 9623034 (2016).
 - [27] L. Yan, Chin. Phys. C **42**, 042001 (2018).
 - [28] S. W. Lan and S. S. Shi, Nucl. Sci. Tech. **33**, no.3, 21 (2022).
 - [29] J. E. Bernhard, J. S. Moreland, S. A. Bass, J. Liu and U. Heinz, Phys. Rev. C **94** no.2, 024907 (2016).
 - [30] B. Schenke, S. Jeon and C. Gale, Phys. Rev. C **82**, 014903 (2010).
 - [31] B. Schenke, S. Jeon and C. Gale, Phys. Rev. Lett. **106** (2011), 042301.
 - [32] I. Karpenko, P. Huovinen and M. Bleicher, Comput. Phys. Commun. **185**, 3016-3027 (2014).
 - [33] E. Molnar, H. Holopainen, P. Huovinen and H. Niemi, Phys. Rev. C **90** no.4, 044904 (2014).
 - [34] P. Bozek and R. Samanta, Phys. Rev. C **105**, no.3, 034904 (2022).
 - [35] K. Xiao, F. Liu and F. Wang, Phys. Rev. C **87**, no.1, 011901 (2013).
 - [36] J. Jia and P. Huo, Phys. Rev. C **90**, no.3, 034915 (2014).
 - [37] J. Jia, P. Huo, G. Ma and M. Nie, J. Phys. G **44**, no.7, 075106 (2017).
 - [38] V. Khachatryan *et al.* [CMS], Phys. Rev. C **92** no.3, 034911 (2015).

- [39] M. Aaboud *et al.* [ATLAS], *Eur. Phys. J. C* **78** no.2, 142 (2018).
- [40] G. Aad *et al.* [ATLAS], *Phys. Rev. Lett.* **126** (2021) no.12, 122301.
- [41] M. Nie [STAR], *Nucl. Phys. A* **1005** , 121783 (2021).
- [42] Gaoguo Yan [STAR], *Quark Matter 2022*, to be published.
- [43] P. Bozek, W. Broniowski and J. Moreira, *Phys. Rev. C* **83**, 034911 (2011).
- [44] P. Bozek and W. Broniowski, *Phys. Rev. C* **97**, no.3, 034913 (2018).
- [45] A. Dumitru, J. Jalilian-Marian, T. Lappi, B. Schenke and R. Venugopalan, *Phys. Lett. B* **706**, 219-224 (2011).
- [46] B. Schenke and S. Schlichting, *Phys. Rev. C* **94**, no.4, 044907 (2016).
- [47] A. Sakai, K. Murase and T. Hirano, *Phys. Lett. B* **829**, 137053 (2022).
- [48] L. G. Pang, G. Y. Qin, V. Roy, X. N. Wang and G. L. Ma, *Phys. Rev. C* **91** no.4, 044904 (2015).
- [49] P. Bozek, W. Broniowski and A. Olszewski, *Phys. Rev. C* **91**, 054912 (2015).
- [50] X. Y. Wu and G. Y. Qin, [arXiv:2109.03512 [hep-ph]].
- [51] A. Behera, M. Nie and J. Jia, *Phys. Rev. Res.* **2**, no.2, 023362 (2020).
- [52] A. Sakai, K. Murase and T. Hirano, *Phys. Rev. C* **102**, no.6, 064903 (2020).
- [53] N. Borghini, P. M. Dinh and J. Y. Ollitrault, *Phys. Rev. C* **63** , 054906 (2001).
- [54] N. Borghini, *PoS LHC07*, 013 (2007).
- [55] N. Borghini, *Eur. Phys. J. C* **30**, 381-385 (2003).
- [56] A. Bzdak and G. L. Ma, *Phys. Rev. C* **97** no.1, 014903 (2018).
- [57] A. Bzdak and G. L. Ma, *Phys. Lett. B* **781** , 117-121 (2018).
- [58] M. T. Xie, G. L. Ma and A. Bzdak, *Phys. Rev. C* **105** no.5, 054904 (2022).
- [59] J. Ze-Fang, Y. Chun-Bin, M. Csanad and T. Csorgo, *Phys. Rev. C* **97** no.6, 064906 (2018).
- [60] S. Acharya *et al.* [ALICE], *Phys. Lett. B* **807**, 135564 (2020).
- [61] L. G. Pang, H. Petersen, G. Y. Qin, V. Roy and X. N. Wang, *Eur. Phys. J. A* **52** no.4, 97 (2016).
- [62] A. Bzdak, V. Koch and J. Liao, *Phys. Rev. C* **83**, 014905 (2011).